Astron. Astrophys. 242, 247–255 (1991)

ASTRONOMY
AND
ASTROPHYSICS

CO observations of southern protoplanetary nebulae with optical counterparts*

V. Bujarrabal and R. Bachiller

Centro Astronómico de Yebes (IGN), Apartado 148, E-19080 Guadalajara, Spain

Received March 8, accepted July 27, 1990

Abstract. We present SEST observations of ^{12}CO and ^{13}CO ($J=2-1$, $1-0$) emission from four southern protoplanetary nebulae presenting bipolar structure in the visible: the Boomerang Nebula, Hen 401, Mz 3 and Roberts 22. ^{12}CO was observed and detected for the first time in all four sources; ^{13}CO emission is also found in the Boomerang Nebula (upper limit presented for Roberts 22). In order to obtain the physical parameters of the nebulae, the observational results are analysed by means of a model of molecular excitation and emission. General properties of the objects, in particular distances and total luminosities, are also rediscussed. Though the analysis of the data is not straightforward, it indicates that objects with higher stellar temperature (and probably more evolved protoplanetary nebulae) tend to present a smaller CO abundance, which is probably due to the photodissociation of molecules by the stellar UV. The total molecular mass of the nebulae is found to range from 0.2 to 0.5 $M_\odot$, the mass loss rates responsible for the nebula formation are therefore high enough to explain the post-AGB evolution of the objects. The ^{13}CO intensity in the Boomerang Nebula is about one half of that of the ^{12}CO line; we argue that the $^{12}CO/^{13}CO$ and $^{12}C/^{13}C$ abundance ratio is probably not larger than 20, similar to those found in other protoplanetary objects.

Key words: interstellar medium: molecules – planetary nebulae – stars: circumstellar matter – stars: late-type

1. Introduction

The transition from red giants to planetary nebulae is probably very fast, and, accordingly, protoplanetary nebulae (PPNe) are rare objects. Only a few objects have been confidently identified as PPNe (see e.g. Bujarrabal et al. 1988); and most of them show indeed quite peculiar properties. Since the central star is often not directly observable, due to the circumstellar extinction, and the molecular gas seems to represent the largest part of the envelope, molecular line studies are of the greatest interest to probe the nature and evolution of PPNe. The molecular emission of the most interesting protoplanetaries observable from the northern hemisphere (OH231.8, CRL2688, CRL618, etc.) has been relatively well studied. However, the total number of PPNe observed in molecular emission is quite small: $\lesssim 10$ probable PPNe have been detected in CO (Bujarrabal et al. 1988), and in most of them the emission is very weak and no other molecule has been found.

Under these conditions, it was obviously necessary to extend the amount of existing molecular data, in particular including among the studied objects those belonging to the southern hemisphere. For such a purpose, we have chosen four PPNe that are relatively well studied at other wavelengths; the knowledge of some general properties of the objects from other observations (that are in fact rediscussed in this paper) allows a detailed study of the cool envelope. The considered objects are the Boomerang Nebula, Hen 401, Mz 3 and Roberts 22; we have detected all of them in CO, the Boomerang Nebula has also been detected in ^{13}CO.

2. Observations

The CO 1.3 mm ($J=2-1$) and 2.6 mm ($J=1-0$) observations were made during September 1–4 with the SEST (for details about the telescope see Olofsson et al. 1988; Booth et al. 1989). The telescope was equipped with a cooled Schottky mixer, system temperatures above atmosphere were of about 500 K at 2.6 mm and 1000 K at 1.3 mm. The FWHP of the antenna is approximately 44″ at 2.6 mm wavelength and 24″ at 1.3 mm. We used an acousto-optical spectrometer, with 720 channels and a channel width of 0.7 MHz. The observations were made in beam-switching or total power mode. Towards the source Roberts 22 the contamination by background (galactic) CO emission was severe. To identify the emission due to the nebula, in this source we made total power observations in which the OFF position was alternatively placed at one beam (FWHP) N, S, E and W around the source. The average of the four different spectra is the increase of the CO emission in the source direction and probably represents the emission of the source itself; this method is known to often produce relatively contamination-free spectra. The detected ^{12}CO ($J=2-1$) line towards Roberts 22 is quite clear (Sect. 4) and confirms the usefulness of the method in this case.

The pointing and calibration were checked by observing standard continuum or line sources. The pointing rms was ~4″, which means that errors (which may be systematic) as large as 8″ are often present; we note that the number of available pointing

Send offprint requests to: V. Bujarrabal

* Based on observations obtained at ESO, La Silla, Chile

sources for the telescope is not large and it was not always possible to find one of them close enough to the object to be observed. These pointing errors have small influence on the calibration of the observations, but obviously affect the mapping at 230 GHz. The observational data in this paper are given in units of main beam brightness temperature (T_{mb}), calculated using values of the main beam efficiency of 0.7 at 2.6 mm and 0.5 at 1.3 mm.

The detected lines are shown in Figs. 1–4, together with predicted profiles (see following sections). The main parameters of the profiles are summarized in Table 1, including comments on the spatial extension of the emission (defined as the region in which the intensity is larger than $\sim 1/3$ of the maximum). In order to calculate these parameters we have smoothed the spectra to a resolution of 1.4 km s^{-1} and gaussian profiles were fitted. Baselines of degree 2–3 were subtracted.

3. Data analysis

As explained above, we have considered four southern objects that were not observed before in molecular emission, but are relatively well known: the Boomerang Nebula, Hen 401, Mz 3 and Roberts 22.

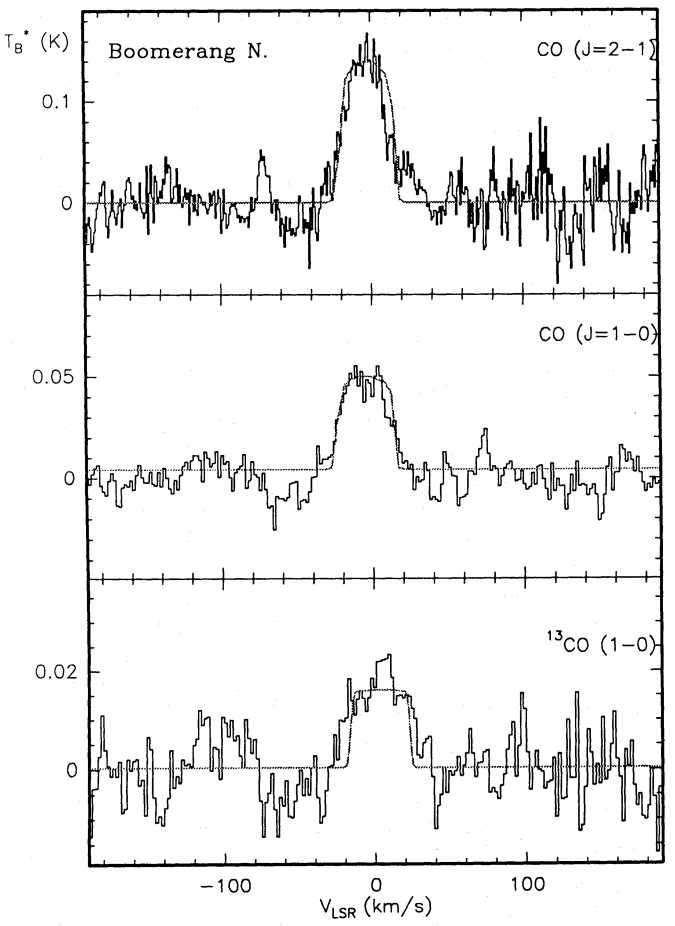

Fig. 1. ^{12}CO $J=2-1$ and $J=1-0$, and ^{13}CO $J=1-0$ emission from the Boomerang Nebula. The grey lines are the profiles predicted by our model calculations (see text)

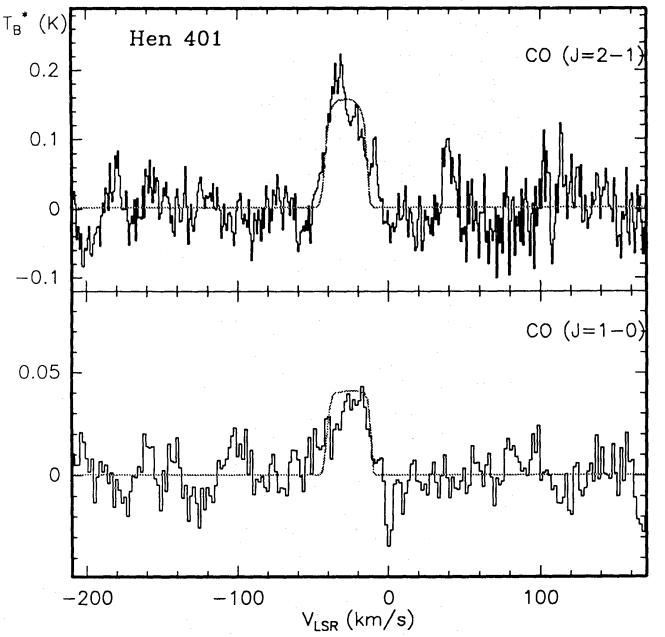

Fig. 2. ^{12}CO $J=2-1$ and $J=1-0$ emission from Hen 401. The grey lines are the profiles predicted by our model calculations (see text)

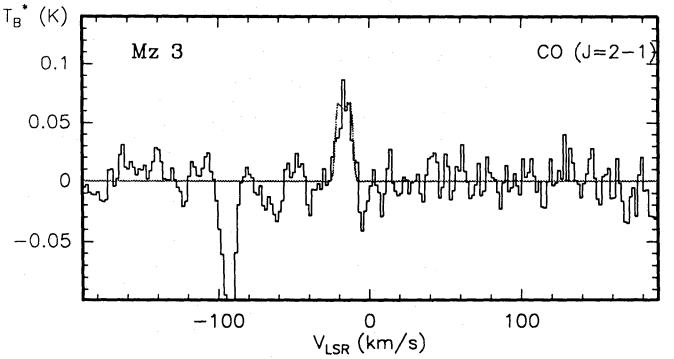

Fig. 3. ^{12}CO $J=2-1$ emission from Mz 3. The grey line is the profile predicted by our model calculations (see text)

In order to improve our analysis of the physical properties of these nebulae, we have considered optical and IR measurements taken from the authors quoted in Sect. 4, the compilation by Gezari et al. (1987) and the IRAS survey (Beichman et al. 1988). The IRAS data were corrected for the color effects by considering for each measurement the colors with respect to the adjacent IRAS wavelengths. The adopted values for the flux densities are presented in Table 2. The total luminosities (ignoring, of course, circumstellar extinction in the visible) were calculated by integrating a linear interpolation of the fluxes. We also considered a short extrapolation, extending the integration limits beyond the first and last wavelength measured by one half of the first and last intervals, respectively; we have verified that the contribution to the total luminosity due to this extrapolation is $\lesssim 5\%$ of the final result for our objects, confirming that the considered spectral range is large enough for our purposes. We note that in all the cases $\gtrsim 50\%$ of the total luminosity is emitted in the FIR (IRAS measurements), and $\gtrsim 90\%$ of this total is found between 2 and

100 μm, which implies a circumstellar extinction in the visible $\gtrsim 3$ mag for the central star's emission. Due to these large extinctions, our method is far more accurate than those often followed in previous studies of our sources, based on the estimation of the optical circumstellar extinction and the correction of the observed V magnitudes.

The distance of the considered objects has been determined by different authors following methods that are not always very reliable (see Sect. 4). Generally more realistic estimates of this parameter can be obtained from the angular size (diameter) of the nebula: as shown by Bujarrabal et al. (1988), the linear sizes of PPNe in the optical are remarkably constant, $\sim 7\,10^{17}$ cm (this property also holds for the extension of the CO emission, at least in the strong emitters). The total dispersion of the calculated sizes of PPNe is only of the order of a factor two for well studied objects; this dispersion takes into account the indetermination of the size due to asymmetries in the nebula shape [the objects considered by Bujarrabal et al. (1988), are in general bipolar, in this case the diameter in the direction of the symmetry axis is used]. Accordingly, we will in general determine the distance by comparing estimates of the angular size with this standard value of the linear size. This method is expected to yield distance values with an error of about a factor of two for our objects, except may be for Roberts 22, for which poor information on its size exists (Sect. 4.4).

The analysis of the observed CO emission has been made by means of a model for CO excitation and emission similar to that presented by Bujarrabal et al. (1989). We note that in our case the details of the inner envelope dynamics (particularly difficult to treat) are not important, since in the considered nebulae the CO emission is expected to come from regions well separated from the star, where the expansion velocity is practically constant. The model includes the calculation of the molecular excitation, using the well known LVG approximation; we only consider small values of the logarithmic velocity gradient, which is taken equal to 0.1 in our LVG code. With the results of the molecular excitation calculations we solve the exact transfer equations and calculate the resulting profile, assuming a constant expansion velocity and a local velocity dispersion of 1.5 km s^{-1}, which was found to be adequate for AGB envelopes (Bujarrabal et al. 1989). A free multiplicative correction smaller than 10% is also considered to account for uncertainties in the calibration and distance.

We assume that our objects present the temperature law used by Bujarrabal et al. for oxygen-rich evolved stars. The thermodynamics of the considered objects is not well known; however, we have verified that variations in the slope of the assumed law of ± 0.3, that means changes in the temperature in most of the envelope by a factor 2–3 with respect to the standard law, can be compensated by moderate changes in the mass loss rate and CO abundance determined from the model fitting (see Bujarrabal et al. 1990). More details about this behaviour are given in Sect. 4 for the case of the Boomerang Nebula, the best studied object of the sample. In envelopes of O-rich AGB stars, a CO abundance $\sim 2\,10^{-4}$ is expected (Bujarrabal et al. 1989), but it is well known that this abundance can be lower in envelopes around more evolved (and hotter) stars, due to the photodissociation by the stellar UV (Bachiller et al. 1988; Bujarrabal et al. 1988). This effect

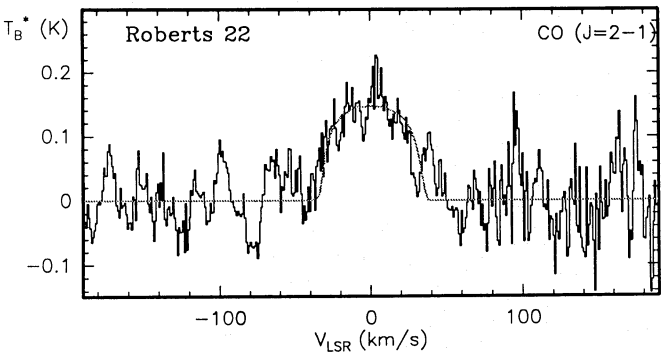

Fig. 4. ^{12}CO $J=2$–1 emission from Roberts 22. The grey line is the profile predicted by our model calculations (see text)

Table 1. Observational data

	T_{mb}(K)	rms (K)	Area (K km s^{-1})	V_c (km s^{-1})	Extension
Boomerang Nebula					
^{12}CO $J=2$–1	0.15	0.02	5.0	−3.5	$\sim 25\times 25''$
^{12}CO $J=1$–0	0.05	0.007	2.0	−5.5	
^{13}CO $J=2$–1		0.07			
^{13}CO $J=1$–0	0.021	0.0055	0.8	3.0	
Hen 401					
^{12}CO $J=2$–1	0.19	0.03	5.2	−29.0	$<20\times 20''$
^{12}CO $J=1$–0	0.04	0.009	1.2	−27.0	
Mz 3					
^{12}CO $J=2$–0	0.06	0.015	0.7	−17.0	
Roberts 22					
^{12}CO $J=2$–1	0.15	0.04	9.0	−0.1	
^{12}CO $J=1$–0	<0.1				
^{13}CO $J=1$–0		0.01			

Table 2. Fluxes (J_ν) of the considered objects at different wavelengths (μm)

	U 0.365	*B* 0.44	*V* 0.55	1.25	1.65	2.2	3.6	4.8	8.6	11	12	25	60	100
Boomerang N	1.9E−3	1.1E−2	3.2E−2	0.11	0.16	0.26	0.6	1.9			5.1	5.9	14.1	16.7
Hen 401		1.7E−2		0.12		0.16					4.2	45.3	79.1	41.5
Mz 3	1.1E−2	2.3E−2	9.7E−3	0.52	1.32	4.50	24.2	27.8	58.0	43.5	103.5	375.5	275.1	111.5
Roberts 22			3.9E−2	0.63	0.92	1.0	2.7		102.8	157.7	223.6	1179.5	576.3	<271.3

is expected to be efficient for PPNe that have left the AGB branch more than $\sim$300 yr ago. Indeed, as we will see, such a decrease in the CO abundance is sometimes necessary to explain the observations, and this parameter must be almost free in the model. The CO photodissociation would affect the distribution in the envelope of the molecule in a way that is difficult to predict; we assume in the calculations that, even in the presence of photodissociation, the CO abundance is uniform in the whole envelope.

In our model we assume spherical symmetry, since no indication of the contrary exists from the molecular data, and the CO envelopes of PPNe are often spherical (Kawabe et al. 1987; Bujarrabal et al. 1988). We note that, since the CO opacities in the analysed objects will not be high, except for Roberts 22, the assumption of spherical symmetry has practically no consequences in the determination of the mass loss rate and CO abundance from the model fitting of the spectra. The external envelope radius R_e is in practice restricted to 3–4 10^{17} cm in our calculations, since in the determination of the distance we will use a standard value of the nebula size; we note that extension measurements of the CO emission in the Boomerang Nebula (4.1) give values comparable to the optical size. We assume small values for the inner envelope radius (R_i), the actual adopted values for this parameter are not important for the total CO emission as long as it remains much smaller than the outer radius. We note that the lack of knowledge on the geometry and the velocity field, as well as other general lacks of the model above discussed, make unlikely an accurate fitting of the profile details (in fact the profiles are not parabolic nor two-peaked, as are for standard AGB envelopes); we will just try to reproduce the main features of the line shape, mainly the width and intensity of the lines. We note that this strongly limits the reach of the model fitting process in order to derive the envelope physical conditions. The predicted profiles are in any case shown superimposed onto the observed ones in Figs. 1 to 4 (grey lines; the velocity center corresponds to that quoted in Table 1).

In the excitation calculations, we take into account the effects of vibrational excitation by dust emission. In the treatment of the vibrational excitation we assume that the IR emission at 5 μm, corresponding to the $v=0\rightarrow1$ CO absorption, comes from a small inner region, with opacities $\lesssim 1$ and relatively high temperatures (800 K), in agreement with the IR observations (Table 2). The size of this region is chosen to be consistent with the observational data. Since the number of available photons for the vibrational excitation is essentially given by the observed flux, the only significant assumption we are making in this treatment is that the emitting region is significantly smaller than the CO cloud. This hypothesis is obviously valid, since the CO cloud is very probably extended up to distances $\gtrsim 10^{17}$ cm from the star, while the observed IR spectra show that the 5 μm emission is produced by hot grains that can be only present at distances $<10^{15}$ cm. Since our objects are not very strong sources at 5 μm, the effect of the vibrational excitation on the microwave molecular emission of the considered nebulae was found to be weak. On the other hand, grain emission at microwave frequencies is too weak to affect the rotational excitation.

In summary, the parameters that remain to be fitted in the model, by comparison with the observed molecular transitions (^{12}CO $J=2$–1, $J=1$–0, ^{13}CO $J=2$–1), are the mass loss rate ($\dot{M}$), the relative CO abundance (X(CO)), the ^{12}CO/^{13}CO abundance ratio, and the expansion velocity (V_e). Note that V_e only depends in fact on the linewidth.

4. Individual objects

4.1. The Boomerang Nebula (IRAS 12419−5414, ESO−172?07)

The Boomerang Nebula (Holmberg et al. 1977; Wegner & Glass 1979; Taylor & Scarrott 1980) is an extended structure composed of two similar lobes that occupies a region of $\Delta\alpha \times \Delta\delta \sim 15'' \times 30''$, it corresponds to two visible regions probably separated by a disk of dusty material located almost parallel to the line of sight. We adopted for the central star the coordinates (1950): R.A. $12^h41^m54.2^s$, dec. $-54°14'47''$. A high polarization of about 60% is detected in the optical continuum from the lobes, perpendicularly to the star's direction, which indicates that the visible structure is mostly due to reflected light from the central object. In the equatorial disc, there is a polarization of 20–50% perpendicular to the lobe direction, probably due to extinction by grains that are aligned in this direction by radiation pressure or a radial magnetic field. Wegner & Glass deduce that the central star is obscured by about $A_V = 2$ mag, due to the circumstellar nebula, and has spectral type G0 III, with $T_{\rm eff} \sim 6000$ K. Like the other objects, the Boomerang Nebula is not physically associated with interstellar molecular clouds or star forming regions.

From the above stellar parameters and the photometric observations by Wegner & Glass (1979), the distance is expected to be ~ 800 pc, and the luminosity would be quite small for a PPNe, $L \sim 30\ L_\odot$. However, the determination of the luminosity and extinction are not very reliable, since it is based in the assumption that the object belongs to one of the standard luminosity classes and is derived from the *U*, *B*, *V* fluxes, which only represent a small fraction of the total luminosity. When the emission in the IR is taken into account (in the way explained above), the calculated total emission is significantly larger than the previous value, $L \sim 84\ L_\odot$. This difference in the total luminosity would imply that the extinction calculated by Wegner & Glass is underestimated by about 1 mag; the surface temperature given by these authors, ~ 6000 K, would also be underestimated by about 1000 K. We also note that the determinations of the luminosity and the distance are not independent, and larger luminosity and distance would also be consistent with the observations. A more realistic estimate of the distance can be obtained assuming that the linear size (diameter) of the nebula is equal to the typical value of this parameter for PPNe (Sect. 3), $\sim 7\ 10^{17}$ cm. The size of the nebula is $\sim 20''$, that would correspond at a distance of 800 pc to $2.4\ 10^{17}$ cm, smaller by a factor of three than the average size of PPNe. If the size of the Boomerang Nebula is imposed to be similar to this average value, a distance of about 2.5 kpc is deduced, and, therefore, a luminosity of $\sim 825\ L_\odot$. In summary, an extinction of $A_V \sim 3$ mag and a luminosity of $L \sim 825\ L_\odot$ seem the better values for these parameters. The stellar luminosity class is then I, and the object would be now placed in the region of the H–R diagram occupied by the other PPNe (e.g. Calvet & Cohen 1978; see Fig. 5).

Our molecular observations show the presence of relatively intense ^{12}CO and ^{13}CO emission (Fig. 1). A quick ten-point map indicates that the emission is extended over a region of $\sim 25'' \times 25''$, similar to the optical extension. Such an extension, as well as the shape and width of the lines, are similar to those usually observed in PPNe, confirming the circumstellar nature of the detected emission. Galactic contamination is not obvious from the observations. The ^{12}CO 2–1 line shows an asymmetry (when compared with the other lines) consisting in a relatively enhanced blue wing. We note that some ripple may be present in the baseline of the CO profiles of this source, we estimate that this effect can introduce an uncertainty of about $\pm 50\%$ in the intensity of the ^{13}CO line.

For a distance of 2.5 kpc, the size of the CO cloud, $\sim 25 \times 25$ arcseconds, corresponds to a radius of $\sim 4\ 10^{17}$ cm. The ^{12}CO $J = 2–1$ and $J = 1–0$ lines can be explained for such a large envelope with mass loss rates of about $2\ 10^{-5}\ M_\odot\ {\rm yr}^{-1}$ and the same high CO abundance as in the envelopes of AGB stars (see discussion above), $X({\rm CO}) \sim 2\ 10^{-4}$. Within the uncertainties, the data may be also fitted by a model with $X({\rm CO}) \sim 10^{-4}$ and $\dot{M} \sim 3\ 10^{-5}\ M_\odot\ {\rm yr}^{-1}$. Note that the stellar temperature is low, hence strong molecular photodissociation it is not expected and the CO abundances must be high. This mass loss rate and the adopted R_e are also consistent with the sizes of the CO cloud deduced from the theory of photodissociation by interstellar UV (Mamon et al. 1988). The expansion velocity is found from the fitting to be $\sim 20\ {\rm km\,s}^{-1}$. The total mass in the cool molecular envelope deduced from the above given parameters is $\sim 0.2\ M_\odot$. The shape of the predicted profiles (Fig. 1), more or less parabolic, is compatible with the observed ones. We note that the observations are still too noisy to allow a precise fitting to the profile; on the other hand, the simple assumptions made in the calculations cannot probably account for the details of the geometry and dynamics of the actual cloud.

One could expect that the temperature law assumed for the molecular envelope of the Boomerang Nebula may overestimate this parameter, since this law was originally derived for the envelopes of Mira variables (Sect. 3) and the luminosity of these stars is usually larger than that of the central star of the Boomerang Nebula. However, as mentioned in Sect. 3, the effect of possible changes in the temperature law on the other physical parameters is small. For instance, if we assume that the logarithmic gradient of the temperature is -1.1, instead of the standard value of -0.9, the CO observations can be fitted with $\dot{M} \sim 5\ 10^{-5}\ M_\odot\ {\rm yr}^{-1}$ and $X({\rm CO}) \sim 8\ 10^{-5}$, values very similar to those found with the standard temperature law. To understand such a behaviour, we must note that the density in most of the nebula is quite low ($\sim 10^2$ cm^{-3}); therefore, the CO lines, that have moderate opacities, present low excitation temperatures. It is well known that under these conditions the molecular line intensity depends on the square density and only slightly on the kinetic temperature (see e.g. Penzias 1974; estimations by means of a two-level model readily confirm this result). The same discussion could be applied for the other nebulae in our sample.

The strong ^{13}CO emission, only about 2.5 times less than the corresponding ^{12}CO line, suggests that the ^{12}CO/^{13}CO abundance ratio may be relatively small. Since the brightness temperature is quite low in both ^{12}CO $J = 2–1$ $J = 1–0$, in spite of the large extension of the source, and the 2–1/1–0 ^{12}CO line ratio is quite high (~ 3), we cannot expect the presence of very large ^{12}CO average opacities in the envelope [see Bujarrabal et al. (1990) for a detailed discussion of a similar case, the envelope of the RV Tau variable R Sct]. It is known that opacity and excitation effects impose the use of a factor (usually > 1) to convert the line ratio into an abundance ratio. However, under these conditions of moderate opacity, it is obvious that such a factor cannot be very large. [As shown by Bujarrabal et al. (1990), using very general arguments, this correction factor is of the order of τ^2, if $\tau > 1$; no significant correction must be applied if $\tau < 1$.] The model calculations confirm this fact, and we deduce the abundance ratio

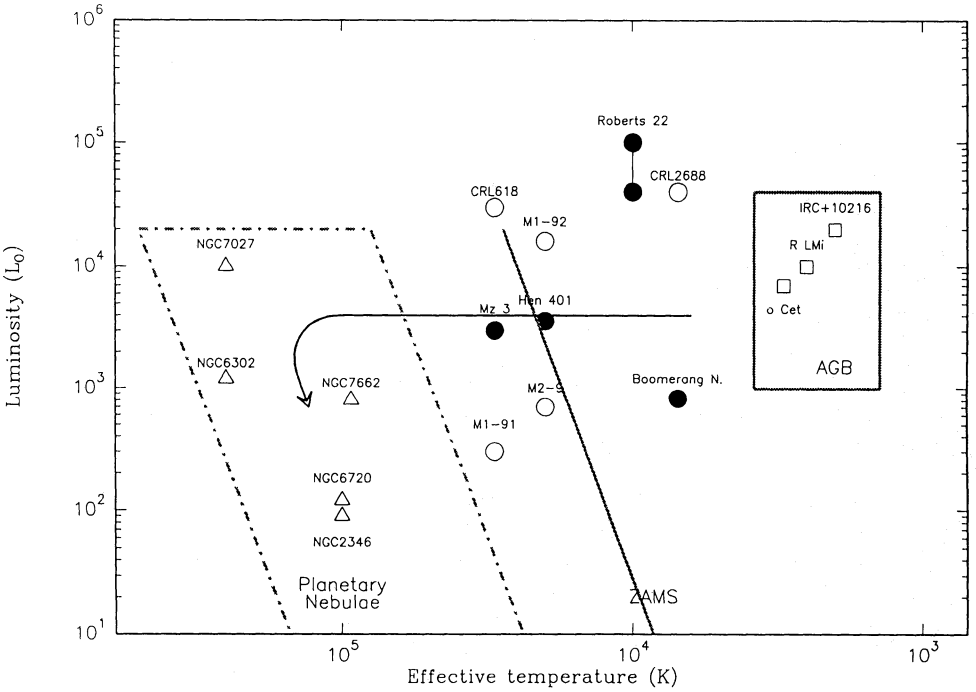

Fig. 5. Localization of the four studied objects (filled circles) in the H–R diagram. Other protoplanetary nebulae (empty circles), AGB stars (squares), planetary nebula (triangles), and the zero-age main sequence are also plotted. The theoretical evolution of a 1 $M_\odot$ protoplanetary (Schönberner 1983) is indicated by the heavy line

$^{12}CO/^{13}CO \sim 5$. Taking into account the uncertainties in the observations and the model (Sect. 3), we will adopt the limit $X(^{12}CO)/X(^{13}CO) < 20$. In order to apply this limit to the $^{12}C/^{13}C$ abundance ratio we must consider the effect of chemical fractionation. In circumstellar envelopes around red giants, fractionation is efficient for CO only in the outer parts of the envelope, where C^+ is abundant enough due to photoionization and the substitution reaction can be efficient. The main effect of fractionation is thus to increase the size of the ^{13}CO cloud (that otherwise would be significantly smaller than the ^{12}CO one due to selective photodissociation; see Mamon et al. 1988; Bujarrabal et al. 1990), approaching the size of the ^{12}CO envelope. No significant increase of the ^{13}CO abundance is expected, even in the outer envelope, with respect to the abundance in the absence of fractionation and selective photodissociation. Note that if the envelope size is smaller for ^{13}CO, our model (in which the envelope radius for both isotopic substitutions is the same) would tend to underestimate the ^{13}CO relative abundance, and the deduced limit would hold a fortiori. Therefore, if these phenomena act in a similar manner for the Boomerang Nebula than for AGB envelopes, the effects of fractionation must be essentially accounted for in the calculations and our limit to the molecular abundance ratio must hold for the $^{12}C/^{13}C$ abundance ratio in the cool envelope of this object.

4.2. Hen 401 (IRAS 10178−5958, Wray 543)

Hen 401 (Sanduleak & Stephenson 1973; Allen 1978) is a reflection nebula of about 25×10 arcsec. The adopted values for the central coordinates (1950) are: R.A. $10^h17^m48.^s$, dec. $-59°58'24''$. The optical spectrum and appearance are similar to those of M1–92 (the Minkowski's Footprint; see Herbig 1975; Calvet & Cohen 1978), therefore, a B1 star ($T_{eff} \sim 22\,000$ K) obscured by $A_V \sim 3$–4 mag is expected. If a distance of 3 kpc is adopted by comparison with M1–92, the integration of the optical and IR data gives a total luminosity of 3600 $L_\odot$.

Our molecular observations show intense ^{12}CO emission at 2.6 and 1.3 mm. No strong galactic contamination is found in the spectra. From a simple 7 point map, an extension smaller than $\sim 20'' \times 20''$ is inferred. The emission appears to peak closer to $\Delta\alpha = +12''$ than to the central map point; however, this can be due to systematic pointing errors somewhat larger than 6″, that we cannot rule out, as explained in Sect. 2.

A model similar to that constructed for the Boomerang Nebula cannot explain the CO observations of Hen 401, since the CO(2–1)/(1–0) intensity ratio is significantly higher in this source, indicating a larger excitation in the CO envelope. The effect of the absorption by the vibrational lines is not enough to explain this high excitation. Therefore, the total density (i.e. the mass loss rate) must be higher; X(CO) must then be smaller than for the Boomerang Nebula, in order to keep the predicted lines as weak as those observed. This is consistent with the higher stellar temperature of Hen 401 and the fact that the CO emission of a similar object like M1–92 is very weak, probably due to photodissociation (Bachiller et al. 1988). In order to get a reasonable fitting to the CO observation, we must change the values of the mass loss rate and abundance at least to $\dot{M} \sim 6\,10^{-5}\,M_\odot\,yr^{-1}$, $X(CO) \sim 3\,10^{-5}$ (note that for larger values of $\dot{M}$ the dependence on the density of the theoretical intensity ratio CO(2–1)/CO(1–0) begins to saturate). We also find for the Hen 401 neutral nebula $R_e \sim 3\,10^{17}$ cm, and $V_e \sim 15$ km s^{-1}. The total molecular mass is deduced to be $\sim 0.4\,M_\odot$ in the cool nebula of Hen 401; comparable to the total mass of the hot bright component of M1-92 (Cohen & Kuhi 1977).

We must note that the value we have given for the mass loss rate of Hen 401 can therefore be considered just as a lower limit, since, as long as we suppose that X(CO) can be significantly smaller than the standard value, we could still decrease X(CO)

and fit the observed intensities with larger values of $\dot{M}$. On the other hand, the quality of the spectra and our knowledge of the geometry and kinematics of the CO nebula are not good enough to undertake a detailed fitting of the profile shapes, that should avoid this indetermination. Nevertheless, we think that the figure given above can be considered a reasonable value for the mass loss rate, more than just a lower limit, since much larger rates would lead to excessively high values for the mass of the envelope.

Since the luminosity of Hen 401 is comparable to that of Miras, the temperature law discussed in Sects. 3 and 4.1 is probably valid for this object. In that case, the differences in the total density and CO abundance found between the Boomerang Nebula and Hen 401 could be partially due to possible differences in temperature between both objects. In any case, this does not affect that Hen 401 seems to be CO deficient with respect to the envelopes of AGB stars and of well studied molecule-rich PPNe (like CRL618 and CRL2688).

4.3. Mz 3 (IRAS 16133−5151, PK 331−1°1)

Mz 3 (Evans & Thackeray 1950; Evans 1959; Cohen et al. 1978; Calvet & Cohen 1978) presents two similar lobes extended in the N–S direction over a region of about 20″ × 50″. We adopted for the central position the coordinates (1950): R.A. $16^h13^m22.3^s$, dec. −51°51′46″. The visible hot (17 000 K) nebula is formed by a rather diffuse gas ($2\,10^3$ cm^{-3}), see Cohen et al. From the excitation of the visible nebula, Cohen et al. deduced that the central star has a spectral type *B*0, with $T_{\rm eff} \sim 30\,000$ K. These authors give a luminosity for Mz 3, $L \sim 6\,10^3\ L_\odot$, for a distance of 1.8 kpc. A circumstellar extinction of about 4 mag in the central regions of the object was deduced from Balmer decrements.

Also in this case, the determination of the distance and total luminosity are not independent. The (relatively large) angular size of the nebula suggests a distance of ∼1 kpc, rather than 1.8 kpc (this variation in the distance would imply an increase by about a 30% in the hot-gas density). Taking into account the flux integral, we deduce a luminosity $L \sim 3\,10^3\ L_\odot$ at a distance of ∼1 kpc; the corresponding correction to the circumstellar extinction calculated by Cohen et al. is small.

The ^{12}CO $J=2-1$ line detected in Mz 3 is very weak. A five-point map of the source suggests that the emission is not extended, though the weakness of the line prevented a reliable estimate of the envelope angular size. The absence of interstellar clouds in this region of the sky with a velocity of -17 km s^{-1} (see the galactic CO survey by Bronfman et al. 1990), also supports the association of the detected emission with Mz 3. Galactic contamination at radial velocity ~ -90 km s^{-1} is however present in the spectra, but with little effect on the observed line.

The CO lines in Mz 3 are by far the weakest of the observed sample. The model fitting of the CO emission, under such conditions of poor observational CO data and little information about the molecular nebula, is very difficult. Mz 3 has the hottest (and probably the most evolved) central star; therefore, the weakness of its molecular emission should be due to the effect of photodissociation by the star's UV radiation. The weakness of the CO line in Mz 3 could also be explained by a very low mass for the envelope, but this would be in contradiction with the fact that the FIR intensity is smaller than that of Hen 401 but larger than that of the Boomerang Nebula (if the distance difference is taken into account), in both cases by about a factor of two. This suggests, assuming reasonable variations in the gas/dust abundance ratio, that the envelope thickness would be comparable in all three objects. We therefore adopt $\dot{M} \sim 3\,10^{-5}\ M_\odot$ yr^{-1} and $R_e = 3.5\ 10^{17}$ cm, and that R_i remains much smaller than R_e. With these parameters, we determine from the model fitting to our observations a CO relative abundance $\sim 0.5\ 10^{-6}$, i.e. more than 100 times smaller than for CO-rich PPNe and for AGB star envelopes. Note that to avoid this small value of the molecular abundance we would have to use a mass loss rate about 100 times smaller than for the Boomerang Nebula and Hen 401, which is certainly incompatible with the IR data. The expansion velocity is $V_e \sim 6$ km s^{-1}.

We note that the photodissociation efficiency of the central star of Mz 3, with 30 000 K surface temperature, can be much larger than that of the central object of Hen 401, with 20 000 K. Firstly, the dissociating far-UV photons are more than ten times more abundant (due to the temperature difference) in Mz 3 than in Hen 401. On the other hand, Bachiller et al. (1988) estimated that a 30 000 K star photodissociates most of the CO of the surrounding nebula in about 300 yr. This time period is of the order of that required by the PPNe evolution to change the surface temperature of the central star from 20 000 to 30 000 K (e.g. Schönberner 1983; Bujarrabal et al. 1988). Since objects with $\lesssim$20 000 K would need significantly more time to dissociate the nebular CO, and in spite of the lack of detailed knowledge on the evolution of PPNe and their central objects, it seems likely to find strong differences in the CO abundance between nebulae with central star temperatures $\gtrsim$30 000 K and $\lesssim$20 000 K.

The adopted parameters correspond to a molecular mass in the nebula $\sim 0.5\ M_\odot$. From the analysis of the radiocontinuum of Mz 3 by Cohen et al. (1978), and assuming a radius of the H II region of 15″ and a distance of 1 kpc, we find a total ionized mass $\sim 0.025\ M_\odot$. On the other hand, a mass of $\sim 0.05\ M_\odot$ can be derived for the inner bright part of the lobes, following the analysis of different spectral lines presented by those authors.

4.4. Roberts 22 (IRAS 10197−5750, CRL 4104, Hen 404, Wray 549, G 284.2−0.8, OH 284.18−0.79)

Roberts 22 (Roberts 1962; Sanduleak & Stephenson 1973; Frogel & Persson 1975; Allen et al. 1980) is a bipolar nebula showing two well separated reflection lobes, that occupy a region of about 10″ × 4″. The central coordinates (1950) are: R.A. $10^h19^m45.0^s$, dec. −57°50′30″. The nebular extinction is thought to be ∼5–10 mag in the average, but larger towards the star, which is not detected to a limit of $m_R \sim 16$ mag (Allen et al. 1980). Sanduleak & Stephenson measured $m_V = 12.5$ mag, probably including the nebular contribution. From the excitation state of the surrounding gas, Allen et al. deduced that the stellar object probably has spectral type A2 I, with a surface temperature of about 10 000 K. Roberts 22 presents strong OH maser emission (Manchester et al. 1969, 1970; Allen et al. 1980) indicating a stellar velocity of -6 km s^{-1} and a circumstellar expansion velocity $V_e \sim 20$ km s^{-1}; strong variability has been detected in the OH emission. Allen et al. (1980) suggest a kinematical distance of 2 kpc and a luminosity of $2\ 10^4\ L_\odot$ (calculated by extrapolation from middle IR data), but recognize that both values are very uncertain.

From the size of the nebula, we deduce a distance of ∼4 kpc, still compatible with a kinematical determination of distance. However, we note that the existing information on the visible size of Roberts 22 is particularly poor, it means that the size given

above is probably a lower limit and, therefore, that the value for the distance of 4 kpc is just an upper limit. Since the circumstellar extinction is very high and the FIR emission of the object is very intense (see Table 2), the only direct way to determine the apparent total luminosity is the integration of the IR fluxes. The integration of the total spectrum leads to a high total luminosity: $L(L_\odot) \sim 6.4\ 10^3\ D^2$, as a function of the distance D(kpc). (Note that the corresponding apparent luminosity and limit to the extinction are not much larger than the values proposed by Allen et al. 1980.) At a distance of 4 kpc, we calculate for Roberts 22, $L \sim 10^5\ L_\odot$, the largest luminosity of the well studied PPNe. For $D = 2$ kpc, $L \sim 3\ 10^4\ L_\odot$.

Our observations show the presence of intense ^{12}CO $J = 2-1$ emission; a galactic feature at the radial velocity range 10–20 km s^{-1} is also found. The spectrum shown in Fig. 4, from which the parameters in Table 1 were deduced, was obtained following the observational procedure described in Sect. 2, which is expected to minimize the effects of an extended galactic component. The situation was much more critical for the 2.6 mm ^{12}CO line (due to the larger size of the beam), the value given in Table 1 for this line is only an estimated upper limit. The fact that the detected emission is spread on a wide velocity range comparable to that observed in OH (Allen et al. 1980) supports the association of the CO line emission with the protoplanetary nebula. The shape of the profile is also similar to that detected in CO in other PPNe (see above) and in many circumstellar envelopes. The detected wide emission does not seem to be spatially extended, but to obtain a quantitative estimate of or limit to the angular extension was impossible due to the contamination.

In spite of the large distance to Roberts 22, the CO emission is quite intense. We assume a distance of 4 kpc, a high CO abundance, since the central star of the nebula is still not very hot, and an external envelope radius of $3.5\ 10^{17}$ cm. With these parameters, we determine a mass loss rate $\dot{M} \sim 10^{-4}\ M_\odot\ \mathrm{yr}^{-1}$ for $X(\mathrm{CO}) = 2\ 10^{-4}$, and $\dot{M} \sim 1.5\ 10^{-4}\ M_\odot\ \mathrm{yr}^{-1}$ for $X(\mathrm{CO}) = 10^{-4}$ (only the first fitting is represented in Fig. 4). These mass loss rates are comparable to the high rates found in objects like CRL 618 and CRL 2688. The expansion velocity determined from the fitting is $V_e \sim 35$ km s^{-1}. The total molecular mass in the nebula for the above parameters is $\sim 0.4\ M_\odot$. Note that the assumption of significantly smaller values of X(CO), for instance similar to that found for Mz 3, would imply anomalously large values of the total nebular mass, of many solar masses, and of the mass loss rate.

5. Conclusions

We have observed millimeter wave emission from ^{12}CO and ^{13}CO in four southern protoplanetary nebulae which are relatively well studied at other wavelengths: the Boomerang Nebula, Hen 401, Mz 3 and Roberts 22.

In order to improve the analysis of these data and our knowledge of the general properties of the objects, we have reanalysed the values of the distances and total luminosities. For such a purpose, we have integrated the optical-IR spectra of the sources. The distance to the objects was also recalculated by means of the standard PPN linear size derived by Bujarrabal et al. (1988) and the angular size of the objects, a method that is more accurate than those previously used for these nebulae. For the stellar temperature T_{eff} we adopted, when it was possible, the values determined from the excitation state of the hot visible nebulae, since this method seems quite reliable. For the Boomerang Nebula we recalculated the value of T_{eff} using the improved value of the extinction and color measurements. The derived values for the distance, total luminosity and stellar temperature are summarized in Table 3. If one knows the values of these parameters, it is possible to place our four objects in a Hertzsprung-Russell diagram (Fig. 5), together with other well known PPNe and some planetaries and AGB stars. It is found that our objects are essentially placed in the same region than the other PPNe, between red giants and planetaries. We have also shown in the figure the theoretical evolutionary track of a 1 $M_\odot$ post-AGB star (from Schönberner 1983). We note the high luminosity of Roberts 22, between 4 and $10\ 10^4\ L_\odot$; the Boomerang Nebula presents the lowest luminosity of the considered objects, $L \sim 800\ L_\odot$, being possibly less massive than the Sun. Note also the low temperature of this object, consistent with it being the least evolved of our nebulae.

The fitting of the observed profiles by means of the model described in Sect. 3 has allowed the calculation of the total mass (M_{mol}) of the cool envelope and the mass loss responsible for its formation ($\dot{M}$), the expansion velocity and the CO abundance (X(CO)). The values of these parameters are listed in Table 3. We have deduced relative abundances of CO ranging from $2\ 10^{-4}$ to $0.5\ 10^{-6}$. High values of X(CO), similar to that characteristic of AGB envelopes, are probably present in the Boomerang Nebula and Roberts 22, the two coolest objects. Mz 3 and, to some extent, Hen 401, seem to be deficient in molecules (with respect to the Boomerang Nebula and Roberts 22, as well as to the envelopes of AGB stars and other protoplanetary nebulae like CRL 2688 and CRL 618). Since both objects have quite hot central stars, this CO underabundance is probably due to an efficient photodissociation of molecules by the stellar UV radiation (Bachiller et al. 1988; Bujarrabal et al. 1988).

As mentioned above, we have also determined the total mass of the cool envelope (M_{mol}). In general, the obtained values can explain the total mass loss necessary to generate, by means of the ejection of an important part of the stellar material, the post-AGB evolution ($M_{\mathrm{mol}} \gtrsim 0.3\ M_\odot$; see e.g. Schönberner 1983). Only in the

Table 3. Derived parameters for the considered objects

	D(kpc)	T_{eff}(K)	$L(L_\odot)$	$\dot{M}(M_\odot\ \mathrm{yr}^{-1})$	X(CO)	$M_{\mathrm{mol}}(M_\odot)$
Boomerang N	2.5	7000	800	2–3E–5	2–1E–4	0.2
Hen 401	3	20000	3.6E3	6E–5	3E–5	0.4
Mz 3	1	30000	3E3	3E–5	5E–7	0.5
Roberts 22	4–2	10000	10–4E4	1E–4	1–2E–4	0.4

Notes: M_{mol} = molecular mass in the nebula; T_{eff} = stellar effective temperature (see text)

Boomerang Nebula, the total nebular mass is relatively small, $\sim 0.2\ M_\odot$. The apparent lack of mass in the molecular envelope of this object cannot be explained by assuming that the amount of ionized gas is very high, since this object is the coolest of the sample. It is probable that the evolution of stars during the PPNe state is triggered by different phases of mass ejection, in such a way that objects that are quite far from the PN stage, like the Boomerang Nebula, must still lose (or have recently lost) large amounts of matter. In this context, we must take into account that shells ejected a short time ago are occupying a too small volume. This small size can make it difficult to detect these shells in CO emission, their mass not being considered in the above estimations, though their contribution to the total extinction and near-IR emission is not negligible. It is to be noted, in any case, that low-luminosity PPNe have in general low-mass molecular envelopes: M2–9 and the Red Rectangle are expected to have $M_{\rm mol} \sim 10^{-2}$–$10^{-1}\ M_\odot$ (Bachiller et al. 1988, 1990), while for CRL 618 and CRL 2688 (Bujarrabal et al. 1988), as well as for the other objects in Table 3, $M_{\rm mol} \sim 0.5\ M_\odot$.

In the Boomerang Nebula we have also detected the ^{13}CO $J=1$–0 line. The ^{13}CO emission is particularly intense, only about 2.5 times less than the corresponding ^{12}CO line. Since the brightness temperature is quite low in both ^{12}CO $J=2$–1 $J=1$–0, in spite of the extension of the envelope, we do not expect the presence of very large ^{12}CO opacities. Therefore, the ^{12}CO/^{13}CO abundance ratio is probably low; as we have shown in Sect. 4.1, $X(^{12}\mathrm{CO})/X(^{13}\mathrm{CO})$ is expected to remain smaller than 20. Assuming that the chemical fractionation effects in our case are comparable to those thought to be present in AGB-star envelopes, we also conclude that this limit holds for the ^{12}C/^{13}C abundance ratio in the cool envelope of the Boomerang Nebula. This result means that the material from which the envelope of this object was formed (probably in a past AGB phase) had been already processed in the star's interior – a similar result is found for the envelope of the RV Tau variable R Sct (Bujarrabal et al. 1990). We note that RV Tau variables are protoplanetary objects with low luminosity and mass ($\sim 0.7\ M_\odot$), and suggest that this high chemical evolution may be a characteristic of the envelopes of low-mass post-AGB objects.

Acknowledgements. We are very grateful to the SEST staff, in particular to Dr. L.Å. Nyman, for their competent support during the observations. We are also indebted to Dr. R. Sahai for critical reading of the manuscript. This work has been partially supported by CICYT, project numbers PB 88-0453 and URC-52/89.

References

Allen D.A., 1978, MNRAS 184, 601
Allen D.A., Hyland A.R., Caswell J.L., 1980, MNRAS 192, 505
Bachiller R., Gómez-González J., Bujarrabal V., Martín-Pintado J., 1988, A&A 196, L5
Bachiller R., Martín-Pintado J., Bujarrabal V., 1990, A&A 227, 188
Beichman C.A., Neugebauer G., Habing H.J., Clegg P.E., Chester T.J., 1988, Infrared Astronomical Satellite (IRAS), Catalogs and Atlases, NASA RP-1190
Booth A.J., Delgado G., Hagström, M., Johansson L.E.B., Murphy D.C., Olberg M., Whyborn N.D., Greve A., Hanson B., Lindström C.O., Rydberg A., 1989, A&A 216, 315
Bronfman L., Alvarez H., Cohen R.S., Thaddeus P., 1990, ApJS 71, 481
Bujarrabal V., Gómez-González J., Bachiller R., Martín-Pintado J., 1988, A&A 204, 242
Bujarrabal V., Gómez-González J., Planesas P., 1989, A&A 219, 256
Bujarrabal V., Alcolea J., Bachiller R., 1990, A&A 234, 355
Calvet N., Cohen M., 1978, MNRAS 182, 687
Cohen M., Kuhi L.V., 1977, ApJ 213, 79
Cohen M., FitzGerald M.P., Kunkel W., Lasker B.M., Osmer P.S., 1978, ApJ 221, 151
Evans D.S., Thackeray A.D., 1950, MNRAS 110, 429
Evans D.S., 1959, MNRAS 119, 150
Frogel J.A., Persson S.E., 1975, ApJ 197, 351
Gezari D.Y., Schmitz M., Mead J.M., 1987, Catalog of Infrared Observations, NASA Reference Publication 1196, NASA Goddard Space Flight Center
Herbig G.H., 1975, ApJ 200, 1
Holmberg E.B., Lauberts A., Schuster H.E., West R.M., 1977, A&AS 27, 295
Kawabe R., Ishiguro M., Kasuga T., Morita K-I., Ukita N., Kobayashi H., Okomura S., Fomalont E.B., Kaifu N., 1987, ApJ 314, 322
Mamon G.A., Glassgold A.E., Huggins P.J., 1988, ApJ 328, 797
Manchester R.N., Goss W.M., Robinson B.J., 1969, Astrophys. Letters 3, 11
Manchester R.N., Robinson B.J., Goss W.M., 1970, Aust. J. Phys. 23, 751
Penzias A.A., 1974, in: Atomic and Molecular Physics and the Interstellar Matter, Les Houches Session XXVI, eds. R. Balian, P. Encrenaz, J. Lequeux, North Holland, Amsterdam
Olofsson H., Eriksson K., Gustafsson B., 1988, A&A 196, L1
Roberts M.S., 1962, AJ 67, 79
Sanduleak N., Stephenson C.B., 1973, ApJ 185, 899
Schönberner D., 1983, ApJ 272, 708
Taylor K.N.R., Scarrott S.M., 1980, MNRAS 193, 321
Wegner G., Glass I.S., 1979, MNRAS 188, 327

Note added in proof: Hen 401 has been independently detected in CO (1–0) by Loup et al. (Loup C., Forveille T., Nyman L.Å, Omont A., 1990, A&A 227, L29).